




# Competition between superconductivity and molecularization in the quantum nuclear behavior of lanthanum hydride

S. van de Bund  and G. J. Ackland \*

Centre for Science at Extreme Conditions and School of Physics and Astronomy, University of Edinburgh,  
EH9 3FD Edinburgh, United Kingdom

 (Received 13 March 2023; revised 28 July 2023; accepted 30 August 2023; published 3 November 2023)

Lanthanum hydride is the superconductor with the highest known critical temperature. It is believed that the superconductivity is of standard BCS type, with electrons forming Cooper pairs and opening the superconducting band gap. Here, we show that the BCS electron pairing is in competition with an alternative pairing: covalent bonding. We show that the covalent pairing is favored at lower pressures, and the superconducting cubic phase becomes unstable as pressure is reduced. Previous calculations based on static relaxation neglect three factors, all of which are important in stabilizing the cubic phase. Finite temperature plays a role, and two quantum effects are also important—the nuclear wave function contributes to destabilizing the  $H_2$  molecules, and the zero-point pressure means that calculated pressures are significantly overestimated by standard methods. We demonstrate these phenomena using Born-Oppenheimer and path-integral molecular dynamics: These give the same qualitative picture, with nuclear quantum effects increasing the transition pressure significantly. This competition between molecularization and superconducting gap formation is the fundamental reason why hydride superconductors have so far been found only at high pressure.

DOI: [10.1103/PhysRevB.108.184102](https://doi.org/10.1103/PhysRevB.108.184102)

## I. INTRODUCTION

It has long been believed that atomic, metallic hydrogen will be a high  $T_c$  superconductor, based on the electron-phonon coupling (BCS) theory [1]. The rationale is that low-mass hydrogen lends itself to high phonon frequencies. The practical difficulty with hydrogen superconductors is that instability against forming Cooper pairs is in competition with a more common pairing effect—molecule formation.

Thus the route to high- $T_c$  superconductivity lies through inhibiting molecule formation. The challenge is to obtain structures where the hydrogen atoms are close enough that the coupling of electrons to hydrogen-dominated phonons is strong, but not so close that the electrons localize into covalent bonds

This can be achieved through very high pressures, by chemical doping, or both. The doping approach can be understood theoretically as adding extra electrons (from cations) to atomic metallic hydrogen to suppress molecule formation and thereby induce superconductivity [2–6]. In many superhydrides,  $H_2$  molecular electron states lie well below the Fermi energy [7]. A third mechanism, symmetry-breaking phonon instabilities, provide another way of lowering the free energy by opening pseudogaps in the electronic band structure at the Fermi energy [8].

Such materials have been made *in situ* in diamond anvil cells by increasing pressure in a hydrogen-rich environment [9]. The first example of this type of superconductor,

hydrogen sulfide, has been well characterized experimentally with a cubic structure, and can be understood theoretically by standard density functional calculations to have composition  $H_3S$  and conventional (BCS) superconductivity [10,11].

There have been a number of recent demonstrations and reports of high-temperature superconductivity in hydrogen-rich compounds at high pressure: The experiments are challenging, and complementary density functional theory calculations (DFT) are essential to determine hydrogen composition and structure. Calculations also demonstrate that high  $T_c$  can arise from conventional (BCS) superconductivity [12–16]. The current experimental record  $T_c$  stands at 250–260 K in a lanthanum hydride, believed to be  $LaH_{10}$  [17,18]. However, a number of issues around understanding this material and how to improve on it remain unresolved [19]. In particular, x-ray diffraction shows that the superconducting phase has a face-centered-cubic ( $Fm\bar{3}m$ ) arrangement of lanthanum atoms [17,18]. However, density functional calculations suggest that  $Fm\bar{3}m$  is unstable to negative-energy phonon distortions primarily involving hydrogen. Such distortions produce infinities in the Migdal-Eliashberg equation and invalidate the BCS approach: The typical theoretical approach is then to ignore the unstable modes [20–24], or to assume the cubic structure is stable and that the unstable mode frequencies can be renormalized [25]. With such approximations, standard BCS calculations of  $T_c$  via density functional theory and the Migdal-Eliashberg equations then suggest a similarly high value for  $T_c$ , agreement with experiment typically being within a factor of 2 [26].

Below 150 GPa,  $Fm\bar{3}m$  DFT calculations suggest that  $LaH_3$  has imaginary phonons throughout the Brillouin zone, and instabilities remain at some points up to 220 GPa [25]. Calculations showing imaginary phonons are not unusual in

\*gjackland@ed.ac.uk

real materials, and are normally linked with temperature-driven phase transitions. Imaginary phonons arise when the curvature of the interatomic potential is negative in some direction: The high-symmetry structure is a saddle point in energy  $E(\{r\})$ . In the Born-Oppenheimer approximation, an imaginary phonon means that the structure is unstable at 0 K. Nevertheless, there may be several nearby energy minima and if temperature is high enough for the system to sample all of these, then the high-symmetry position may also be the average one, as observed in experiment. In addition to temperature, the nuclear quantum effect (NQE) zero-point motion to the hydrogen atoms may be sufficient to escape a shallow potential minimum. Indeed, a perturbative approach to zero-point energy, the stochastic self-consistent harmonic approximation, was applied to LaH<sub>10</sub> and shown to eliminate all instabilities [25,27].

Here, we investigate LaH<sub>10</sub> with DFT forces and both Born-Oppenheimer (BOMD) and path-integral molecular dynamics (PIMD) to determine the phase stability. We find both methods show two distinct states, molecular and atomic transitions. The atomic state is favored at high temperature and pressure. Furthermore, NQEs significantly favor the atomic phase, and make a significant contribution to the calculated pressure.

## II. CALCULATIONS

### A. Path-integral molecular dynamics

Hydrogen molecules have very high vibrational frequency, such that zero-point energy can play a critical role in molecular stability and ambient [28] and even very high temperature [29]. Having identified a molecular phase as stable in a standard DFT calculation, at variance with experiment, it is natural to ask whether NQEs are important, either in shifting the boundary or creating a “quantum crystal structure” [25].

PIMD treats all the nuclei as quantum particles. It is a precise method for calculating the nuclear wave function. PIMD samples the density matrix (finite-temperature nuclear wave function) using a set of coupled classical BOMD simulations (“beads”), connected by springs. In the Copenhagen interpretation, a given bead represents a possible outcome of a measurement of all atomic positions. Each hydrogen atom position is delocalized due to thermal and quantum broadening, which are represented by a combination of classical motion within a bead, and the spread of positions of the atom across different beads (radius of gyration). Even at 300 K, the radius of gyration of hydrogen—a measure of quantum broadening—is found to be at least  $\sim 0.15$  Å, comparable with thermal effects. Note that the electron-phonon coupling arises only through the connections between beads, so the explicit BCS coupling terms are absent and the condensation of Cooper pairs cannot occur.

The PIMD runs were performed using the I-PI code [30] together with QUANTUM ESPRESSO [31]. Sixteen beads were used for the 300 K isotherm, and 20 beads for the 200 K isotherm. A constant stress ensemble was employed with a stochastic path-integral Langevin equation local thermostat (PILE\_L) thermostat [32] and anisotropic stochastic barostat [33] as implemented in I-PI, in order to allow for changes in the cell vectors.

In contrast to the BOMD, we find that at low pressures the PIMD shows a distinctive covalent bonding peak at 50 GPa (see Figs. 1 and 2). For 300 K, at pressures of 75 GPa and higher, the PIMD ensemble-averaged structure adopts the highly symmetric  $Fm\bar{3}m$  structure, even though transient bonding occurs within each bead. The additional NQE together with the thermal contribution is likely sufficient to overcome the imaginary modes that lead to distortions in the zero temperature structures—the behavior is otherwise qualitatively similar to the classical nuclei BOMD, but shifted by  $\sim 100$  GPa.

At 200 K, radial distribution functions are very similar to 300 K, and the transition also occurs between 50 and 75 GPa. This near vertical  $dP/dT$  Clapeyron slope is in contrast to the classical simulations. The third law of thermodynamics requires a vertical Clapeyron slope close to  $T = 0$  K, close meaning at temperatures where zero-point motion dominates, rather than classical motion (see Fig. 3).

The quantum effects in LaH<sub>10</sub> can be separated into two parts: the effect on pressure and the effect on structure. Figure 4 shows that for a given volume, the pressure calculated by PIMD is typically 20 GPa lower than for classical simulation. This “zero-point pressure” means that all previous DFT calculations have overstated the pressure to which their results apply, independent of structural details. In addition to this, the zero-point energy favors the atomic form over the molecular one, so when considering the atomic-molecular transformation quantum effects drive it to even lower pressures.

### B. Born-Oppenheimer molecular dynamics

Born-Oppenheimer molecular dynamics treats all the nuclei as classical particles. It is much faster than PIMD, and its role here is to check finite-size effects,  $k$ -point sampling, and the effect of different exchange-correlation functionals. These are also properties which should be converged on each bead of PIMD, since the electronic structure calculation at each bead is equivalent to a BOMD calculation.

BOMD samples the full potential surface, unlike anharmonic lattice dynamics which implicitly represents the potential as a Taylor expansion about a predetermined average structure. By sampling the phase space, BOMD correctly incorporates all classical entropy effects, and explicitly ignores all quantum effects. Thus we can disentangle quantum and classical effects, and determine whether  $Fm\bar{3}m$  LaH<sub>10</sub> can be described classically, or is truly a “quantum crystal”.

Our simulations are done using the CASTEP code [36] with the same *de facto* standard PBE exchange-correlation functional [37] used for PIMD and previous studies [25,28]. We used the  $NPT$  ensemble with a Nose-Hoover thermostat [38], cell-quench equilibration [39], and a constant-stress Parrinello-Rahman barostat [40]. We used cubic La<sub>32</sub>H<sub>320</sub> supercells at a range of pressures and temperatures. Convergence testing shows that  $k$ -point sampling of at least  $3 \times 3 \times 3$  is required, to avoid the MD moving to structures which are tuned to the  $k$ -point set. Obtaining quantitative accuracy for the atomic-molecular transition in hydrogen is particularly challenging for DFT, because the exchange-correlation functional must give a good description of both atomic and covalent hydrogen. PBE tends to form overly weak

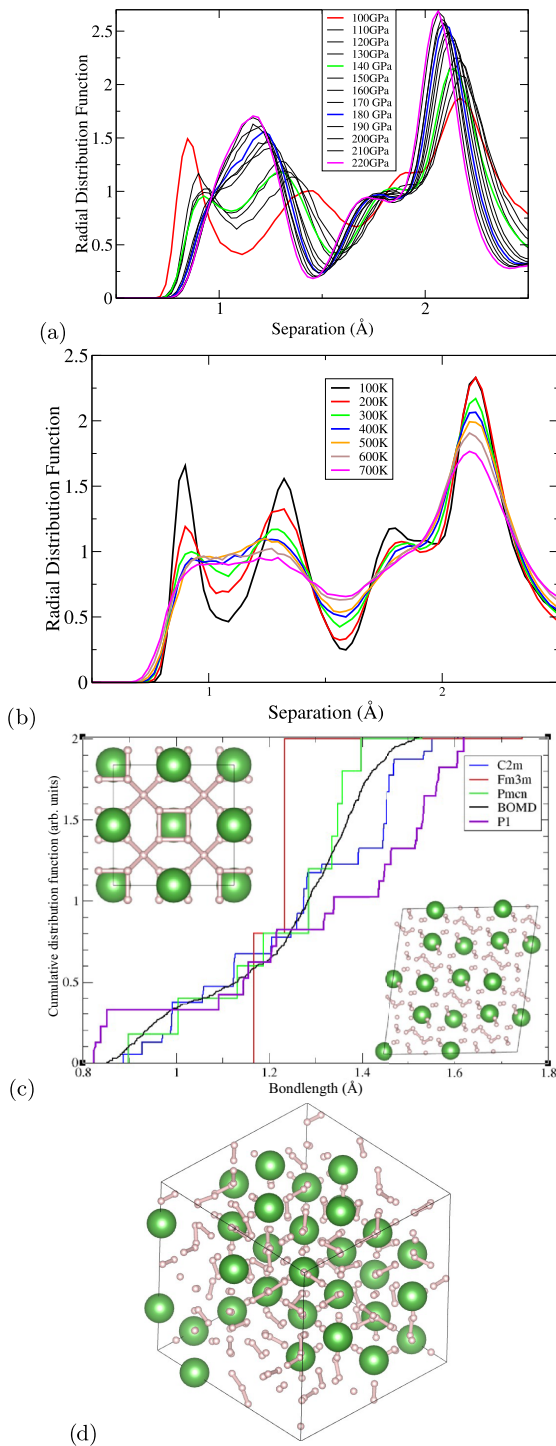


FIG. 1. (a) Radial distribution function (RDF) from BOMD at 300 K, 10 GPa intervals from 100 to 220 GPa with selected pressures highlighted with thicker, colored lines. These show the continuous change from molecular to atomic hydrogen as the first two coordination shells merge. (b) Radial distribution function from BOMD at various temperatures and 140 GPa. The large peak above 2 Å is from H-La. (c) Cumulative distribution function (HH pairs per H atom) for the three static relaxed structures with  $Fm\bar{3}m$ ,  $Pbcn$ , and  $C2m$  symmetry, and one relaxation from a large BOMD snapshot. Insets show structures at 150 GPa  $Fm\bar{3}m$  (“HH bond lengths” less than 1.6 Å shown) and  $P1$   $La_4H_{12}(H_2)_{14}$  (“HH bonds” less than 1.0 Å). (d) Relaxed snapshot from 150 GPa  $NPT$  ensemble MD run.

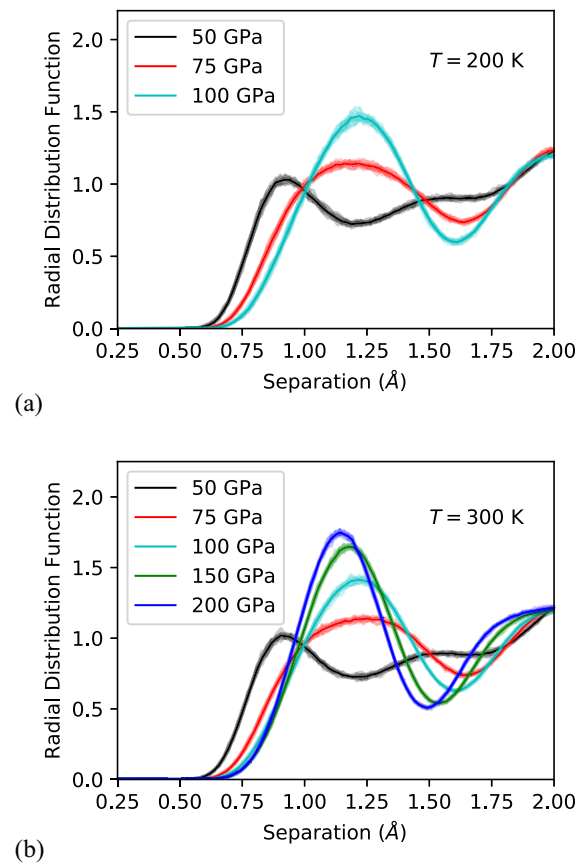


FIG. 2. Radial distribution functions from PIMD at 200 K, 300 K, and various pressures. Solid areas indicate the minimum and maximum extent of the RDF across all beads, and can be thought of as the resulting uncertainty due to NQE.

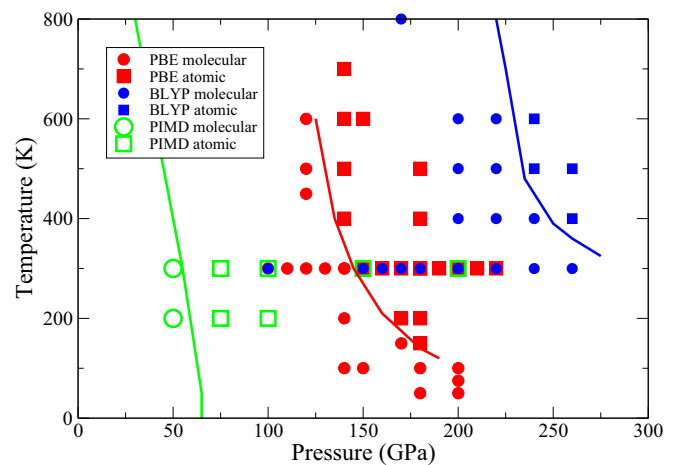


FIG. 3. Phase diagram between atomic (square) and molecular (circular) hydrogen phases. A molecular phase is defined by the existence of a first peak in RDF below 1 Å. Three methods are applied: BOMD-PBE (Perdew-Burke-Ernzerhof) (red) PIMD-PBE (green), and BOMD-BLYP (Becke-Lee-Yang-Parr) (blue) functionals. Only the quantum PIMD calculations are subject to the third law, and therefore have a vertical phase boundary at  $T \rightarrow 0$  K.

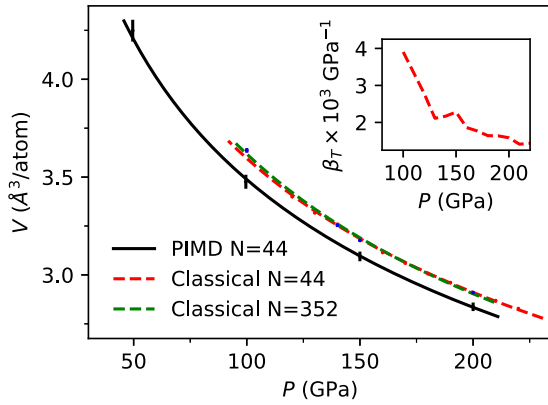


FIG. 4. Comparison of equation of state (EOS) between PIMD and BOMD at 300 K, showing the resulting pressure shift. Lines are obtained with a Vinet EOS fit [34]. For comparison, the experimental volume at 175 GPa is  $3 \text{ \AA}^3/\text{atom}$  [18]. EOS from static relaxations, and using BLYP, showing 30–40 GPa larger pressures at equal volume, are given in the Supplemental Material [35]. Inset: Compressibility of BOMD calculation for 44 atoms at 300 K, showing the peak at 150 GPa corresponding to the transition from molecular to atomic.

$\text{H}_2$  bonds, and to test sensitivity to the exchange-correlation functional we repeated the calculations with the BLYP functional [41,42], which has the opposite tendency [43,44]. Simulations were run as static relaxations and at 300 K and pressures between 50 and 220 GPa.

These large simulations are augmented by smaller 44-atom BOMD, the same size and with identical  $k$ -point sampling grid as in the BOMD runs as used in PIMD: These show good agreement with their larger counterparts, indicating that the PIMD calculations are also converged with system size.

The mean-squared displacement of atoms plateaus at a low value, and the variation of lattice parameters remains broadly unchanged. By contrast, the radial distributions functions (as shown in Fig. 1) show a strong change in the bonding. At lower pressures, e.g., 100 GPa, there is a distinctive peak at 0.85 Å, characteristic of covalently bonded molecular hydrogen. This is not simply an anharmonic phonon distortion from  $Fm\bar{3}m$ —it represents a complete change in the nature of the bonding. As pressure is increased, the bond gets longer. At 150 GPa, the “bond” peak is merely a shoulder.

BOMD can also explore phase transitions in the La sublattice, although for  $\text{LaH}_{10}$  the high La mass makes exploring that phase space impractical. Hence, we use BOMD with fictitious masses ( $M_{\text{La}} = 2M_{\text{H}}$ ) and  $NPT$  ensemble to better sample the equilibrium phase space at the expense of correct dynamics. We found that at all pressures, structures with the La atoms close to  $Fm\bar{3}m$  remain stable. However, the transition from molecular to atomic hydrogen manifests as a distinct peak in the compressibility (Fig. 4), indicating a two-state system rather than a continuous weakening of bonds [45].

### C. Static relaxation

In previous work we have shown that molecular superhydrides tend to obey the “octet rule”: An  $\text{XH}_n$  hydride will typically contain  $(n-x)/2$  molecules, where  $x$  is the

valence of cation  $X$ . For trivalent La, it means that  $\text{LaH}_{10}$  should contain 3.5  $\text{H}_2$  molecules per lanthanum [7]. Static relaxations of snapshots from our BOMD simulations show structures with well-defined molecules. Figure 1(b) illustrates the salient features of these static structures by plotting the number of HH pairs in the cell per hydrogen, as a function of the pair separation. In these units the octet-rule compound  $\text{LaH}_3(\text{H}_2)_{3.5}$  would have a cumulative distribution function (CDF) of 0.35 at the hydrogen bond length. The lowest-energy structure we found from 44-atom MD with the BLYP functional has precisely this, with 14 well-defined  $\text{H}_2$  units and La remaining close to fcc positions (initially  $P1$ , relaxing to  $P2_1/c$ ). Considering previously reported structures, all are less stable, below 150 GPa, and all break the octet rule. In  $Fm\bar{3}m$  there are no short HH distances; a large group appears around 1.2 Å.

In BOMD with the PBE functional, the molecules break more often than with BOMD. At 150 GPa a lower enthalpy is obtained by distorting in a way to create molecules with H-H separation.  $Pm\bar{c}n$  symmetry generates four equivalent sites, so even with a quadrupled unit cell a fractional number of objects (e.g., 3.5  $\text{H}_2$ 's) is forbidden. In fact, the 44-atom  $C2m$  structures form eight covalent-style bonds (0.898 Å, 0.95 Mulliken population) and eight more  $\text{H}_2$  pairs (1.004 Å, 0.70 $e$ ), arguably  $\text{LaH}_2(\text{H}_2)_4$ . Further symmetry breaking to  $C2m$  [46] finds another solution to the incompatibility between charge and stoichiometry,  $\text{H}_3^-$  units:  $\text{La}_4^{3+}\text{H}_{10}^-(\text{H}_3^-)_2(\text{H}_2)_{12}$ .

An important feature of the BLYP calculation is that the density is significantly lower than for PBE, by about 7%, similar in magnitude to the quantum nuclear effects. This equates to about 40 GPa and gives some indication of the uncertainty in DFT calculations. There is no *a priori* reason to prefer one functional over another, so we regard these discrepancies as the uncertainty associated with treating  $\text{LaH}_{10}$  with DFT.

### D. Phase diagram

In Fig. 3, we show the “phase diagram” separating the atomic and molecular “phases,” defined by the presence or absence of a peak in the radial distribution function below 1 Å. The main feature of note is the extreme sensitivity both to quantum effects and to choice of functional. The shift due to quantum motion is close to 100 GPa, of which about 20 GPa comes from the different equation of state, and the rest from the zero-point energy destabilizing the molecules. The choice of functional has an effect of similar magnitude.

Thus the classical DFT situation reflects conventional chemistry, with the  $\text{LaH}_{10}$  stoichiometry demanding large unit cells to satisfy the octet rule with  $\text{La}^{3+}$ ,  $\text{H}^-$ , and  $\text{H}_2$ . Relaxations from the 352-atom MD simulation gave similar patterns, molecule formation with no obvious symmetry, and would induce small distortions in the La sublattice which may be detectable using x-ray diffraction [6,46].  $Fm\bar{3}m$  has special symmetry positions which indicate a specific  $\text{LaH}_{10}$  stoichiometry, but the low symmetry of the molecular phase has no such constraints.

There is therefore no reason why  $\text{LaH}_{10}$  would be the favored stoichiometrically: Any value for  $x$  in  $\text{LaH}_3(\text{H}_2)_x$  can be expected to form octet-rule compounds, the most stable being dependent in theory on the chemical potential of hydrogen,

and in practice on the details of sample preparation. Indeed, no fewer than seven different  $\text{LaH}_3(\text{H}_2)_x$  stoichiometries were recently synthesized at pressures below the atomic-molecular transition [6].

### III. DISCUSSION AND CONCLUSIONS

In summary, we have shown that including quantum nuclear effects in DFT calculations on  $\text{LaH}_{10}$  shifts the calculated pressure of transformation from a molecular/metallic to atomic/superconducting structure to lower pressures. Classical calculations suggest that increasing temperature has a similar effect, favoring the atomic phase which has a higher entropy, however, below room temperature PIMD shows no thermal effect. We ascribe this to the third law, which reduces the significance of entropy at low temperatures in quantum systems. A classical BOMD simulation does not obey the third law.

At finite temperature, molecularlike and atomiclike hydrogen coexist in  $\text{LaH}_{10}$ . Indeed, the formation and breaking of bonds can be viewed as a strong coupling between electronic and ionic degrees of freedom, as required for superconductivity in BCS theory.

There is also considerable dependence on the exchange-correlation functional. PBE and BLYP are regarded as limiting cases for describing hydrogen, so our work implies an uncertainty about the transition pressure of almost 100 GPa in this and in previous DFT calculations. Some of this difference arises simply from the pressure calculations, but most of it can be ascribed to the greater stabilization of molecules by BLYP [43,44,47].

It may seem counterintuitive that the quantum effects, which “spread” the nuclear positions, nevertheless increase the density. Looking at the static relaxation, we find that at a given pressure the fcc (atomic) form is typically denser than the  $P1$  (molecular) form. Our interpretation of this is that the PIMD calculation causes the system to form a more atomiclike state than the BOMD, so fewer molecules in PIMD mean that the density is higher. Such unusual behavior is typical of systems where the components have two possible states [45] and we expect it to be present in all superhydrides close to the atomic-molecular transition.

Perhaps our most wide-ranging result is that the BCS superconducting phase of  $\text{LaH}_{10}$  is in competition with molecularization, a feature which appears to be true in many high-pressure hydrides [7]. Molecular phases have lower energy, but also lower density and entropy. This competition between molecular and atomic forms of hydrogen always favors the molecular form at low pressures. This explains why the high- $T$  superhydride superconductors found to date require high pressure.

### ACKNOWLEDGMENTS

We acknowledge the support of studentship funding from EPSRC under Grant ref EP/L015110/1 and the ERC project HECATE for funding. We are grateful for computational support from the UK national high performance computing service, ARCHER, via the UKCP consortium and funded by EPSRC Grant ref EP/P022561/1. For the purpose of open access, the authors have applied a Creative Commons Attribution (CC BY) licence to any Author Accepted Manuscript version arising from this submission.

- 
- [1] N. W. Ashcroft, Metallic hydrogen: A high-temperature superconductor? *Phys. Rev. Lett.* **21**, 1748 (1968).
- [2] N. W. Ashcroft, Hydrogen dominant metallic alloys: High temperature superconductors? *Phys. Rev. Lett.* **92**, 187002 (2004).
- [3] E. Zurek, R. Hoffmann, N. Ashcroft, A. R. Oganov, and A. O. Lyakhov, A little bit of lithium does a lot for hydrogen, *Proc. Natl. Acad. Sci. USA* **106**, 17640 (2009).
- [4] F. Peng, Y. Sun, C. J. Pickard, R. J. Needs, Q. Wu, and Y. Ma, Hydrogen clathrate structures in rare earth hydrides at high pressures: Possible route to room-temperature superconductivity, *Phys. Rev. Lett.* **119**, 107001 (2017).
- [5] E. Zurek and T. Bi, High-temperature superconductivity in alkaline and rare earth polyhydrides at high pressure: A theoretical perspective, *J. Chem. Phys.* **150**, 050901 (2019).
- [6] D. Laniel, F. Trybel, B. Winkler, F. Knoop, T. Fedotenko, S. Khandarkhaeva, A. Aslandukova, T. Meier, S. Chariton, K. Glazyrin *et al.*, High-pressure synthesis of seven lanthanum hydrides with a significant variability of hydrogen content, *Nat. Commun.* **13**, 6987 (2022).
- [7] M. Marques, M. Peña-Alvarez, M. Martinez-Canales, and G. J. Ackland,  $\text{H}_2$  chemical bond in a high-pressure crystalline environment, *J. Phys. Chem. C* **127**, 15523 (2023).
- [8] G. J. Ackland and I. R. Macleod, Origin of the complex crystal structures of elements at intermediate pressure, *New J. Phys.* **6**, 138 (2004).
- [9] M. I. Eremets, V. S. Minkov, A. P. Drozdov, P. Kong, V. Ksenofontov, S. I. Shylin, S. L. Bud’ko, R. Prozorov, F. F. Balakirev, D. Sun *et al.*, High-temperature superconductivity in hydrides: experimental evidence and details, *J. Supercond. Novel Magn.* **35**, 965 (2022).
- [10] A. P. Drozdov, M. I. Eremets, I. A. Troyan, V. Ksenofontov, and S. I. Shylin, Conventional superconductivity at 203 K at high pressures, *Nature (London)* **525**, 73 (2015).
- [11] I. Errea, M. Calandra, C. J. Pickard, J. Nelson, R. J. Needs, Y. Li, H. Liu, Y. Zhang, Y. Ma, and F. Mauri, High-pressure hydrogen sulfide from first principles: A strongly anharmonic phonon-mediated superconductor, *Phys. Rev. Lett.* **114**, 157004 (2015).
- [12] M. Kostrzewa, K. Szcześniak, A. Durajski, and R. Szcześniak, From  $\text{LaH}_{10}$  to room-temperature superconductors, *Sci. Rep.* **10**, 1592 (2020).
- [13] C. J. Pickard, I. Errea, and M. I. Eremets, Superconducting hydrides under pressure, *Annu. Rev. Condens. Matter Phys.* **11**, 57 (2020).
- [14] B. Chen, L. J. Conway, W. Sun, X. Kuang, C. Lu, and A. Hermann, Phase stability and superconductivity of lead hydrides at high pressure, *Phys. Rev. B* **103**, 035131 (2021).
- [15] W. Sun, X. Kuang, H. D. J. Keen, C. Lu, and A. Hermann, Second group of high-pressure high-temperature lanthanide polyhydride superconductors, *Phys. Rev. B* **102**, 144524 (2020).

- [16] K. P. Hilleke and E. Zurek, Tuning chemical precompression: Theoretical design and crystal chemistry of novel hydrides in the quest for warm and light superconductivity at ambient pressures, *J. Appl. Phys.* **131**, 070901 (2022).
- [17] A. Drozdov, P. Kong, V. Minkov, S. Besedin, M. Kuzovnikov, S. Mozaffari, L. Balicas, F. Balakirev, D. Graf, V. Prakapenka *et al.*, Superconductivity at 250 K in lanthanum hydride under high pressures, *Nature (London)* **569**, 528 (2019).
- [18] M. Somayazulu, M. Ahart, A. K. Mishra, Z. M. Geballe, M. Baldini, Y. Meng, V. V. Struzhkin, and R. J. Hemley, Evidence for superconductivity above 260 K in lanthanum superhydride at megabar pressures, *Phys. Rev. Lett.* **122**, 027001 (2019).
- [19] V. Struzhkin, B. Li, C. Ji, X.-J. Chen, V. Prakapenka, E. Greenberg, I. Troyan, A. Gavriluk, and H.-k. Mao, Superconductivity in La and Y hydrides: Remaining questions to experiment and theory, *Matter Radiat. Extremes* **5**, 028201 (2020).
- [20] C. Wang, S. Yi, and J.-H. Cho, Pressure dependence of the superconducting transition temperature of compressed LaH<sub>10</sub>, *Phys. Rev. B* **100**, 060502(R) (2019).
- [21] D. A. Papaconstantopoulos, M. J. Mehl, and P.-H. Chang, High-temperature superconductivity in LaH<sub>10</sub>, *Phys. Rev. B* **101**, 060506(R) (2020).
- [22] C. R. Kwang-Hua, Superconducting at 298.2 K in lanthanum hydrides, *Mater. Lett.* **271**, 127743 (2020).
- [23] I. A. Kruglov, D. V. Semenok, H. Song, R. Szczesniak, I. A. Wrona, R. Akashi, M. M. Davari Esfahani, D. Duan, T. Cui, A. G. Kvashnin, and A. R. Oganov, Superconductivity of LaH<sub>10</sub> and LaH<sub>16</sub> polyhydrides, *Phys. Rev. B* **101**, 024508 (2020).
- [24] S. F. Elatresh, T. Timusk, and E. J. Nicol, Optical properties of superconducting pressurized LaH<sub>10</sub>, *Phys. Rev. B* **102**, 024501 (2020).
- [25] I. Errea, F. Belli, L. Monacelli, A. Sanna, T. Koretsune, T. Tadano, R. Bianco, M. Calandra, R. Arita, F. Mauri *et al.*, Quantum crystal structure in the 250-kelvin superconducting lanthanum hydride, *Nature (London)* **578**, 66 (2020).
- [26] Better agreement is often reported, but this can be traced to tweaking of undetermined parameters in the model.
- [27] F. Belli, T. Novoa, J. Contreras-García, and I. Errea, Strong correlation between electronic bonding network and critical temperature in hydrogen-based superconductors, *Nat. Commun.* **12**, 5381 (2021).
- [28] Y. Watanabe, T. Nomoto, and R. Arita, Quantum and temperature effects on the crystal structure of superhydride LaH<sub>10</sub>: A path integral molecular dynamics study, *Phys. Rev. B* **105**, 174111 (2022).
- [29] S. van de Bund, H. Wiebe, and G. J. Ackland, Isotope quantum effects in the metallization transition in liquid hydrogen, *Phys. Rev. Lett.* **126**, 225701 (2021).
- [30] V. Kapil, M. Rossi, O. Marsalek, R. Petraglia, Y. Litman, T. Spura, B. Cheng, A. Cuzzocrea, R. H. Meißner, D. M. Wilkins, B. A. Helfrecht, P. Juda, S. P. Bienvenue, W. Fang, J. Kessler, I. Poltavsky, S. Vandenbrande, J. Wieme, C. Corminboeuf, T. D. Kühne *et al.*, i-PI 2.0: A universal force engine for advanced molecular simulations, *Comput. Phys. Commun.* **236**, 214 (2019).
- [31] P. Giannozzi, O. Andreussi, T. Brumme, O. Bunau, M. B. Nardelli, M. Calandra, R. Car, C. Cavazzoni, D. Ceresoli, M. Cococcioni, N. Colonna, I. Carnimeo, A. D. Corso, S. de Gironcoli, P. Delugas, R. A. DiStasio, Jr., A. Ferretti, A. Floris, G. Fratesi, G. Fugallo *et al.*, Advanced capabilities for materials modelling with Quantum Espresso, *J. Phys.: Condens. Matter* **29**, 465901 (2017).
- [32] M. Ceriotti, M. Parrinello, T. E. Markland, and D. E. Manolopoulos, Efficient stochastic thermostating of path integral molecular dynamics, *J. Chem. Phys.* **133**, 124104 (2010).
- [33] M. Ceriotti, J. More, and D. E. Manolopoulos, i-PI: A Python interface for *ab initio* path integral molecular dynamics simulations, *Comput. Phys. Commun.* **185**, 1019 (2014).
- [34] P. Vinet, J. R. Smith, J. Ferrante, and J. H. Rose, Temperature effects on the universal equation of state of solids, *Phys. Rev. B* **35**, 1945 (1987).
- [35] See Supplemental Material at <http://link.aps.org/supplemental/10.1103/PhysRevB.108.184102> for additional results on the functional sensitivity of the EOS, along with convergence testing and the electronic density of states (DOS).
- [36] S. J. Clark, M. D. Segall, C. J. Pickard, P. J. Hasnip, M. J. Probert, K. Refson, and M. C. Payne, First principles methods using CASTEP, *Z. Kristallogr.* **220**, 567 (2005).
- [37] J. P. Perdew, K. Burke, and M. Ernzerhof, Generalized gradient approximation made simple, *Phys. Rev. Lett.* **77**, 3865 (1996).
- [38] S. Nose, Constant-temperature molecular dynamics, *J. Phys.: Condens. Matter* **2**, SA115 (1990).
- [39] G. J. Ackland, Rapid equilibration by algorithmic quenching the ringing mode in molecular dynamics, *MRS Adv.* **1**, 2857 (2016).
- [40] M. Parrinello and A. Rahman, Polymorphic transitions in single crystals: A new molecular dynamics method, *J. Appl. Phys.* **52**, 7182 (1981).
- [41] A. D. Becke, Density-functional exchange-energy approximation with correct asymptotic behavior, *Phys. Rev. A* **38**, 3098 (1988).
- [42] C. Lee, W. Yang, and R. G. Parr, Development of the Colle-Salvetti correlation-energy formula into a functional of the electron density, *Phys. Rev. B* **37**, 785 (1988).
- [43] R. C. Clay III, J. Mcminis, J. M. McMahon, C. Pierleoni, D. M. Ceperley, and M. A. Morales, Benchmarking exchange-correlation functionals for hydrogen at high pressures using quantum Monte Carlo, *Phys. Rev. B* **89**, 184106 (2014).
- [44] S. Azadi and G. J. Ackland, The role of van der Waals and exchange interactions in high-pressure solid hydrogen, *Phys. Chem. Chem. Phys.* **19**, 21829 (2017).
- [45] G. J. Ackland, H. Zong, V. N. Robinson, S. Scandolo, and A. Hermann, Two-state model for critical points and the negative slope of the melting curve, *Phys. Rev. B* **104**, 054120 (2021).
- [46] Z. M. Geballe, H. Liu, A. K. Mishra, M. Ahart, M. Somayazulu, Y. Meng, M. Baldini, and R. J. Hemley, Synthesis and stability of lanthanum superhydrides, *Angew. Chem.* **130**, 696 (2018).
- [47] G. J. Ackland and I. B. Magdău, Appraisal of the realistic accuracy of molecular dynamics of high-pressure hydrogen, *Cogent Phys.* **2**, 1049477 (2015).